PAPER • OPEN ACCESS

Bethe ansatz approach for dissipation: exact solutions of quantum many-body dynamics under loss

New Journal of Physics
The open access journal at the forefront of physics

Deutsche Physikalische Gesellschaft DPG
IOP Institute of Physics

Published in partnership with: Deutsche Physikalische Gesellschaft and the Institute of Physics

OPEN ACCESS

RECEIVED
2 November 2020

REVISED
30 November 2020

ACCEPTED FOR PUBLICATION
7 December 2020

PUBLISHED
23 December 2020

PAPER

Bethe ansatz approach for dissipation: exact solutions of quantum many-body dynamics under loss

Berislav Buča[1,*], **Cameron Booker**[1], **Marko Medenjak**[2] **and Dieter Jaksch**[1]

[1] Clarendon Laboratory, University of Oxford, Parks Road, Oxford OX1 3PU, United Kingdom
[2] Institut de Physique Théorique Philippe Meyer, École Normale Supérieure, PSL University, Sorbonne Universités, CNRS, 75005 Paris, France
[*] Author to whom any correspondence should be addressed.

E-mail: berislav.buca@physics.ox.ac.uk

Keywords: open quantum systems, integrability, Bethe ansatz, Heisenberg spin chains, domain wall

Abstract

We develop a Bethe ansatz based approach to study dissipative systems experiencing loss. The method allows us to exactly calculate the spectra of interacting, many-body Liouvillians. We discuss how the dissipative Bethe ansatz opens the possibility of analytically calculating the dynamics of a wide range of experimentally relevant models including cold atoms subjected to one and two body losses, coupled cavity arrays with bosons escaping the cavity, and cavity quantum electrodynamics. As an example of our approach we study the relaxation properties in a boundary driven *XXZ* spin chain. We exactly calculate the Liouvillian gap and find different relaxation rates with a novel type of dynamical dissipative phase transition. This physically translates into the formation of a stable domain wall in the easy-axis regime despite the presence of loss. Such analytic results have previously been inaccessible for systems of this type.

1. Introduction

Particle loss is an important mechanism of environmental dissipation. It strongly affects the dynamics of many particle systems in the classical and quantum regimes and has an immense impact on technological applications. It is present in numerous experimental platforms including cold atoms [1, 2], non-linear waveguides [3], coupled cavity arrays [4–7], THz cavities [8–11], quantum wires [12, 13], condensed matter systems [14], and solid-state devices [15]. Indeed, the primary source of dissipation in these settings is a consequence of particles escaping from the system either through one- or two-body processes [2], or due to the coupling to an external electromagnetic field (e.g. [4, 8, 15]). The platforms underlie future quantum technologies, which will require efficient manipulation of many constituents.

Understanding the behaviour of such systems is of paramount importance, and sheds light on properties that are robust to dissipation and could therefore allow for more efficient methods of information storage and the development of novel error correction mechanisms. However, due to the exponential complexity, numerical simulations of these systems are challenging. Thus, gaining a better understanding of their properties through uncovering their analytical structure is highly desirable. Thus far, exact solutions of such systems have been limited only to the stationary states of boundary driven systems [16–35] and to those with non-interacting Hamiltonians [36–57]. Beyond this only certain approximate methods [58–62], e.g. introducing dissipation on hydrodynamical scales, are available.

In this letter we go beyond these results and develop an analytic approach to describing the dynamics of a wide class of fully interacting dissipative systems. Our approach opens a novel avenue for the analytical study of experimentally relevant many-body models experiencing loss, provided that the system's effective non-Hermitian Hamiltonian is integrable. In experimental settings, examples of systems treatable by our method can be found in cold atom quantum simulators subjected to single and two body losses [1, 2, 8], and driven-dissipative cavity arrays of bosons [4].

As an example of the power of our method we study the instructive and paradigmatic *XXZ* spin chain, often used to describe limiting cases of the aforementioned experimental setups [2], which we subject to boundary spin loss. We find that our model exhibits intriguing physical phenomena. Additionally, these types of localized loss processes recently attracted a lot of theoretical and experimental interest due to their importance for understanding transport properties and as an experimentally realistic venue for preparing interesting quantum states, see e.g. [3, 12, 13, 16, 30, 34, 63–72].

Using our method we first characterize the relaxation dynamics, uncovering a dynamical dissipative phase transition [73, 74], by calculating the closure of the Liouvillian gap. Next, we analytically show the presence of a novel type of dynamical dissipative phase transition that corresponds to non-analyticity in many relaxation rates beyond the leading decay mode. Physically this implies a transition in the dynamics on both short and asymptotic time scales. This should be contrasted with phase transitions in the stationary state [75–78] or the leading decay mode [73]. In our case the stationary state is always the same and a phase transition occurs in the leading decay mode *and* in other parts of the spectrum. Related to this, we show that a stable domain wall state is formed in the easy-axis regime. Interestingly, the domain wall formation occurs spontaneously if the system is initialized in the maximally polarized state. It arises as a consequence of boundary bound states that we solve for. Formation of domain walls in both integrable and non-integrable closed systems has also recently attracted considerable interest [79–83], but is currently still analytically unsolved.

2. Solving lossy models

We will focus on systems described by the Lindblad master equation which characterizes open quantum systems in the weak system-bath coupling limit. The dynamics of the density matrix ρ is provided by the generator $\mathcal{L}$ as [84, 85],

$$\frac{\mathrm{d}}{\mathrm{d}t}\rho(t) = \hat{\mathcal{L}}\rho(t) := -\mathrm{i}[H,\rho(t)] + \sum_{\mu}\left(2L_{\mu}\rho(t)L_{\mu}^{\dagger} - \{L_{\mu}^{\dagger}L_{\mu},\rho(t)\}\right), \tag{1}$$

where H is the system Hamiltonian and L_μ are the Lindblad jump operators modeling the influence of the environment on the system. The time evolution of an observable O can be computed by diagonalizing the generator $\hat{\mathcal{L}}$,

$$\langle O(t)\rangle = \mathrm{tr}(O\rho(t)) = \sum_{\mu} \mathrm{e}^{\lambda_\mu t}\,\mathrm{tr}(\tilde{\rho}_{\mu}^{\dagger}\rho(0))\mathrm{tr}(\rho_{\mu}O), \tag{2}$$

where λ_μ are the eigenvalues and $\rho_\mu, \tilde{\rho}_\mu$ the right and left eigenvectors.

The general setup that we consider comprises an integrable Hamiltonian H with a conservation law M and Lindblad operators L_μ that change the eigenvalue of M by well-defined amounts $m_\mu > 0$, $[M, L_\mu] = -m_\mu L_\mu$, inducing the loss of the quantity M in the system. For instance M can be the total particle number and L_μ particle annihilation operators. In the following we will discuss the integrability requirements for applying our technique. The Liouvillian superoperator can be represented on the vector space with doubled degrees of freedom by the channel-state transformation $|\psi\rangle\langle\phi| \to |\psi\rangle \otimes |\phi\rangle$, yielding

$$\hat{\mathcal{L}} = -\mathrm{i}(H\otimes\mathbb{1} - \mathbb{1}\otimes H^{\mathrm{T}}) + +\sum_{\mu}\left(2L_{\mu}\otimes L_{\mu}^{*} - L_{\mu}^{\dagger}L_{\mu}\otimes\mathbb{1} - \mathbb{1}\otimes(L_{\mu}^{\dagger}L_{\mu})^{\mathrm{T}}\right). \tag{3}$$

We will show that in order to obtain eigenvalues of the Liouvillian it suffices to obtain eigenvalues E_j of the non-Hermitian Hamiltonian $\tilde{H} \equiv -\mathrm{i}H - \sum_\mu L_\mu^\dagger L_\mu$ [86, 87]. Since $[\tilde{H}, M] = 0$, we can assume that the eigenvectors $|\psi_j\rangle$ of $\tilde{H}$ are also eigenvectors of M. The generator (3) can now be decomposed into two parts

$$\hat{\mathcal{L}} = \mathcal{H} + \mathcal{D}, \tag{4}$$

with $\mathcal{H} \equiv \tilde{H}\otimes\mathbb{1} + \mathbb{1}\otimes\tilde{H}^{*}$ and $\mathcal{D} = 2\sum L_\mu \otimes L_\mu^*$. Since $\mathcal{H}$ is a sum of two operators acting on the factors in a tensor product independently, its eigenvalues read $\mathcal{H}|\psi_i\rangle\otimes\overline{|\psi_j\rangle} = (E_i + E_j^*)|\psi_i\rangle\otimes\overline{|\psi_j\rangle}$. Let us now order the eigenvectors $|\psi_i\rangle\otimes\overline{|\psi_j\rangle}$ of $\mathcal{H}$ by the corresponding eigenvalues $m_{i,j}$ of $\mathcal{M} \equiv M\otimes\mathbb{1} + \mathbb{1}\otimes M$. Due to the purely lossy dynamics the nondiagonal matrix elements of $\mathcal{D}$ lie strictly above the diagonal. This immediately implies that $\hat{\mathcal{L}}$ takes the upper triangular form in the basis $|\psi_i\rangle\otimes\overline{|\psi_j\rangle}$ and that the eigenvalues of the Liouvillian $\lambda_{i,j} = E_i + E_j^*$ coincide with those of $\mathcal{H}$. Thus, provided that the non-Hermitian Hamiltonian $\tilde{H} = -\mathrm{i}H - \sum_\mu L_\mu^\dagger L_\mu$ is exactly solvable, we have found the full spectrum of the Liouvillian. However, the structure of Liouvillian eigenvectors corresponding to the eigenvalue $\lambda_{i,j}$ is more complicated and includes the states $|\psi_k\rangle\otimes\overline{|\psi_l\rangle}$, with $m_{k,l} \leqslant m_{i,j}$ as demonstrated in appendix A. Note that the dynamics describing pure gain can be treated on the same footing.

For general interacting, many-body systems, solving $\tilde{H}$ is still intractable due to the exponential complexity. However, we will now outline how Bethe ansatz techniques [88, 89] may be employed to solve $\tilde{H}$ in a wide range of models. In many physically relevant situations the dissipative contribution, $\sum_\mu L_\mu^\dagger L_\mu$, modifying the system's integrable Hamiltonian, H, will leave $\tilde{H}$ integrable. For instance, single particle bulk loss throughout the system in *any* integrable model with particle number conservation, the dissipative contribution corresponds simply to the particle number operator, which clearly implies integrability of $\tilde{H}$. For two-level systems with conserved magnetization the L_μ would correspond to on-site spin lowering operators. This is known to be a primary dissipative loss mechanism in numerous experimental setups such as optical lattices (due to interactions with the background vacuum), wave guides, solid state contacts, and coupled cavity arrays [2–4, 15]. Other examples of dissipative mechanisms that preserve integrability of $\tilde{H}$ are provided by nearest-neighbour dissipation [90, 91] and two-body loss processes [2, 92]. Further details are provided in the following section which demonstrate the wide utility and applicability of our technique.

It is instructive to contrast this situation with cases where the full Liouvillian can be mapped to a non-Hermitian integrable Hamiltonian [49–51, 53, 54, 56, 57] (where the physical system's Hamiltonian is quadratic). In our case the system's Hamiltonian is interacting and the full Liouvillian does not necessarily correspond to some non-Hermitian integrable Hamiltonian. Rather here it is only $\tilde{H}$ (and hence $\mathcal{H}$ in equation (4)) that is integrable.

We now provide further explicit details of the possible models where our technique can be applied before demonstrating the utility of our method we by focusing on the example of the Heisenberg *XXZ* chain in the presence of a spin sink at a single boundary.

3. Examples of dissipative quantum models solvable by Bethe ansatz

Every integrable system Hamiltonian offers at least one corresponding lossy dissipative process that renders it solvable according to our approach. Here we detail such examples.

3.1. Localized loss on two sides

A direct generalization of the loss studied in the main text is putting a loss process on the other side of the chain. This could be done for instance by studying the 1D Hubbard model,

$$H = -t\sum_{j,\sigma}\left(c_{j,\sigma}^\dagger c_{j+1,\sigma} + c_{j+1,\sigma}^\dagger c_{j,\sigma}\right) + U\sum_i n_{j\uparrow}n_{j\downarrow}. \tag{5}$$

We then study four Lindblad operators $L_{1/2} = \sqrt{\gamma_1}c_{1,\downarrow/\uparrow}$, $L_{1/2} = \sqrt{\gamma_2}c_{N,\downarrow/\uparrow}$. The Liouvillian is triangular and,

$$\tilde{H} = -\mathrm{i}H - \sum_{\sigma\in\{\uparrow,\downarrow\}}\gamma_1 n_{1,\sigma} + \gamma_2 n_{N,\sigma}, \tag{6}$$

which is integrable [93]. Of course, the Hubbard model is just a concrete example—any other boundary integrable model would work here, too.

3.2. Single body loss

Take any integrable $U(1)$ symmetric Hamiltonian with symmetry $N = \sum_j a_j^\dagger a_j$, and corresponding loss $L_k = \gamma a_k$, $[N, a_k] = -a_k$. We have immediately that,

$$\tilde{H} = -\mathrm{i}H - \gamma N, \tag{7}$$

which is trivially integrable.

3.3. Two-body loss

Consider the Lieb–Liniger model of cold bosons,

$$H = \int \mathrm{d}x\left[-\Psi(x)^\dagger\partial_x^2\Psi(x) + c\Psi^\dagger(x)\Psi^\dagger(x)\Psi(x)\Psi(x)\right], \tag{8}$$

a very experimentally relevant loss process is two-body loss [1, 2, 94],

$$\hat{\mathcal{L}}\rho = -\mathrm{i}[H,\rho] + \gamma\int \mathrm{d}x\left[2\Psi^2(x)\rho\Psi^{\dagger 2}(x) - \{\Psi^{\dagger 2}(x)\Psi^2(x),\rho\}\right]. \tag{9}$$

This may be understood as a continuous set of Lindblad operator $L(x) = \sqrt{\gamma}\Psi^2(x)$ inducing pure loss. This leads to the triangular form the Liouvillian required. Furthermore,

$$\tilde{H} = -\mathrm{i}\int \mathrm{d}x \left[-\Psi(x)^\dagger \partial_x^2 \Psi(x) + (c - \mathrm{i}\gamma)\Psi^\dagger(x)\Psi^\dagger(x)\Psi(x)\Psi(x)\right], \tag{10}$$

which is a modification of the interaction leaving $\tilde{H}$ integrable. Another concrete physical example of two-body loss treatable with our method is the 1D Hubbard model with two-body recombination of fermions of spin-down and spin-up [92].

3.4. Dissipative lossy nearest-neighbour hopping

A very related loss process is the following. Consider again the *XXZ* spin chain described by H from the main text with $L_j = \sqrt{\gamma}\sigma_j^- \sigma_{j+1}^-$ with $j = 1, \ldots, N-1$. In that case $\hat{\mathcal{L}}$ is again triangular and,

$$\tilde{H} = -\mathrm{i}H - \sum_{j=1}^{N-1} \frac{\gamma}{4}(\mathbb{1} + \sigma_j^z)(\mathbb{1} + \sigma_{j+1}^z), \tag{11}$$

which is again integrable because it corresponds up to an irrelevant constant to an addition of constant magnetic field and boundary field. It also renders the Δ complex. This is interesting from the point of quantum phases because it allows for a physically motivated reason to extend the already rich quantum phase diagram of the *XXZ* spin chain to complex Δ. This is similar to two-level systems coupled by dipolar interactions and subject to nonlocal dissipation, i.e. decay through optical emissions [90, 91].

3.5. Collective loss process

Collective loss process are quite ubiquitous from the point of view of descriptions of cavity experiments (e.g. [95–99]) and Bose–Einstein condensates (BECs) (e.g. [100, 101]). As an example we will take the Bose–Hubbard dimer [102–105],

$$H = k(N_1 - N_2)^2 - \nu(N_1 - N_2) + \mu(N_1 + N_2) - \epsilon(b_1^\dagger b_2 + b_2^\dagger b_1), \tag{12}$$

which has the total particle number $U(1)$ symmetry and is exactly solvable via Bethe ansatz [106, 107]. We now take global loss $L = \sqrt{\gamma}(b_1 + b_2)$, which leaves the Liouvillian triangular, and the non-Hermitian Hamiltonian is just $\mathrm{i}H$ with $\mu \to \mu - \mathrm{i}\gamma$ and $\epsilon \to \epsilon - \mathrm{i}\gamma$. Other possible examples of models with collective loss may include Richardson–Gaudin models [108].

4. Boundary driven *XXZ* spin chain dynamics

We now study the example of an *XXZ* spin-1/2 chain with a single boundary spin sink. Our method allows us to analytically find the scaling of the Liouvillian gap and to understand the formation of domain walls in the easy-axis regime via boundary bound states which we can solve for.

4.1. Dissipative Bethe ansatz solution

The Heisenberg Hamiltonian reads

$$H_{XXZ} = \sum_{j=1}^{N-1} \sigma_j^x \sigma_{j+1}^x + \sigma_j^y \sigma_{j+1}^y + \Delta \sigma_j^z \sigma_{j+1}^z, \tag{13}$$

where the Pauli spin-$\frac{1}{2}$ operators are $\sigma^{x,y,z}$, Δ is the anisotropy, and N is the number of spin sites. We study the setup with an arbitrary loss rate on the first site $L_1 = 2\sqrt{\Gamma}\sigma_1^-$. The corresponding non-Hermitian Hamiltonian reads

$$\tilde{H} = -\mathrm{i}H_{XXZ} - 2\Gamma\sigma_1^z - 2\Gamma\mathbb{1}, \tag{14}$$

i.e. $\mathrm{i}\tilde{H}$ describes an *XXZ* spin chain Hamiltonian in the presence of an imaginary magnetic field at the boundary. The Hamiltonian has a $U(1)$ symmetry $M = \sum_j \sigma_j^z$ and $[M, L_1] = -L_1$, i.e. $m_1 = 1$.

In contrast to boundary driven spin chains [16–18, 36, 109–113] the stationary state, $\hat{\mathcal{L}}\rho_\infty = 0$, is not of interest in our system since it is a trivial vacuum state. However, we obtain the full spectrum of the non-Hermitian Hamiltonian equation (14), and therefore of the Liouvillian[3] by the Bethe ansatz. The Bethe

[3] The Liouvillian itself does not seem to be mappable to any known integrable non-Hermitian Hamiltonian. We checked this by performing vectorization and then attempting to solve a reflection equation that would generate the Liouvillian, but it proved impossible. The spectral statistics cannot be used to check for integrability because the spectrum of the Liouvillian is the same as that of the integrable non-Hermitian Hamiltonian.

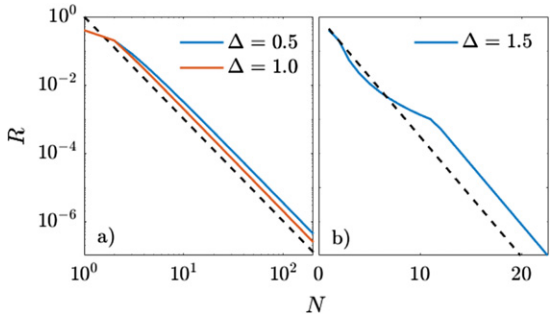

Figure 1. Scaling of the Liouvillian gap, R, with system size for $\Gamma = 0.1$. (a) Power law closing of the gap for $\Delta \leqslant 1$ with $R \propto 1/N^3$ (dashed line) shown for comparison. (b) Exponential closing of the gap for $\Delta > 1$ with $R \propto \Delta^{-2N}$ (dashed line) shown for comparison.

equations were obtained using Sklyanin's reflection algebra [114], and equivalently the coordinate Bethe ansatz [89, 115–117] with imaginary boundary magnetic field $2\mathrm{i}\Gamma\sigma_1^z$.

The complex energies of $\tilde{H}$ corresponding to m magnons read

$$E(\{k_j\}) = -\mathrm{i}(N-1)\Delta - 4\mathrm{i}\sum_{j=1}^{m}(\cos(k_j) - \Delta), \tag{15}$$

where the momenta of the magnons, $\{k_j\}$, are obtained by solving the Bethe equations

$$\frac{\mathrm{e}^{2\mathrm{i}Nk_j}(\Delta - \mathrm{e}^{\mathrm{i}k_j})(\mathrm{e}^{\mathrm{i}k_j} + 2\mathrm{i}\Gamma - \Delta)}{(\mathrm{e}^{\mathrm{i}k_j}\Delta - 1)(1 + \mathrm{e}^{\mathrm{i}k_j}(2\mathrm{i}\Gamma - \Delta))} = \prod_{l\neq j}^{m} S(\mathrm{e}^{\mathrm{i}k_j}, \mathrm{e}^{\mathrm{i}k_l}). \tag{16}$$

The scattering matrix of two magnons takes the form

$$S(a,b) = \frac{(a - 2\Delta ab + b)(1 - 2\Delta a + ab)}{(a - 2\Delta + b)(1 - 2\Delta b + ab)}. \tag{17}$$

From the triangular form of the Liouvillian, which couples different magnetization sectors, we can express its eigenstates in terms of Bethe states of $\tilde{H}$ by simplified Gaussian elimination (for details see appendix A). For later convenience we introduce a pair of labels $(m_\mathrm{L}, m_\mathrm{R})$ re the eigenstferring toates of $\hat{\mathcal{L}}$ comprised of tensor product of two Bethe states with m_L and m_R magnons as well as tensor products of Bethe states with less $q_\mathrm{L} < m_\mathrm{L}$ and $q_\mathrm{R} < m_\mathrm{R}$ magnons. In what follows we will utilise our results to address two physically interesting questions.

4.2. Eigenvalue structure and the Liouvillian gap

The first problem that we consider is the Liouvillian gap, R, of $\hat{\mathcal{L}}$. It corresponds to the maximum real part of the eigenvalues different from 0, which is the inverse relaxation time of the longest-lived eigenmodes. We plot it in figure 1 for different values of the anisotropy parameter Δ. The scaling of the gap with the system size N is one of the primary features of open quantum systems, governing the late time dynamics.

We observe numerically that the gap corresponds to the eigenstates of $\hat{\mathcal{L}}$ with $m_\mathrm{L} + m_\mathrm{R} = 1$. By examining the single magnon $m = 1$ solutions of (16) on top of the steady state we find that the gap closes at different rates depending on the value of Δ. In particular, we demonstrate that for $\Delta \leqslant 1$ the longest lived excitations correspond to the solutions with $\lim_{N\to\infty} \Im(k_j) = 0$, while for $\Delta > 1$ they correspond to solutions with $\lim_{N\to\infty} \Im(k_j) = -\log(\Delta)$.

We find that the real part of the eigenvalue with the smallest (non-zero) real part scales as[4],

$$R = \begin{cases} -\dfrac{1}{N^3}\dfrac{8\pi^2\Gamma}{4\Gamma^2 + (\Delta+1)^2} + o\left(\dfrac{1}{N^3}\right), & \Delta \leqslant 1 \\ -\dfrac{1}{\Gamma}\dfrac{(\Delta^2-1)^3}{\Delta^2}\Delta^{-2N} + o(\Delta^{-2N}), & \Delta > 1 \end{cases}. \tag{18}$$

The result for $\Delta \leqslant 1$ matches the scaling of the gap for free fermions [39].

[4] See appendix B for details. Strictly speaking this is an upper bound on the gap because there could possibly be slower decay modes outside the single magnon sector, but extensive numerical calculations confirm that we find the correct value.

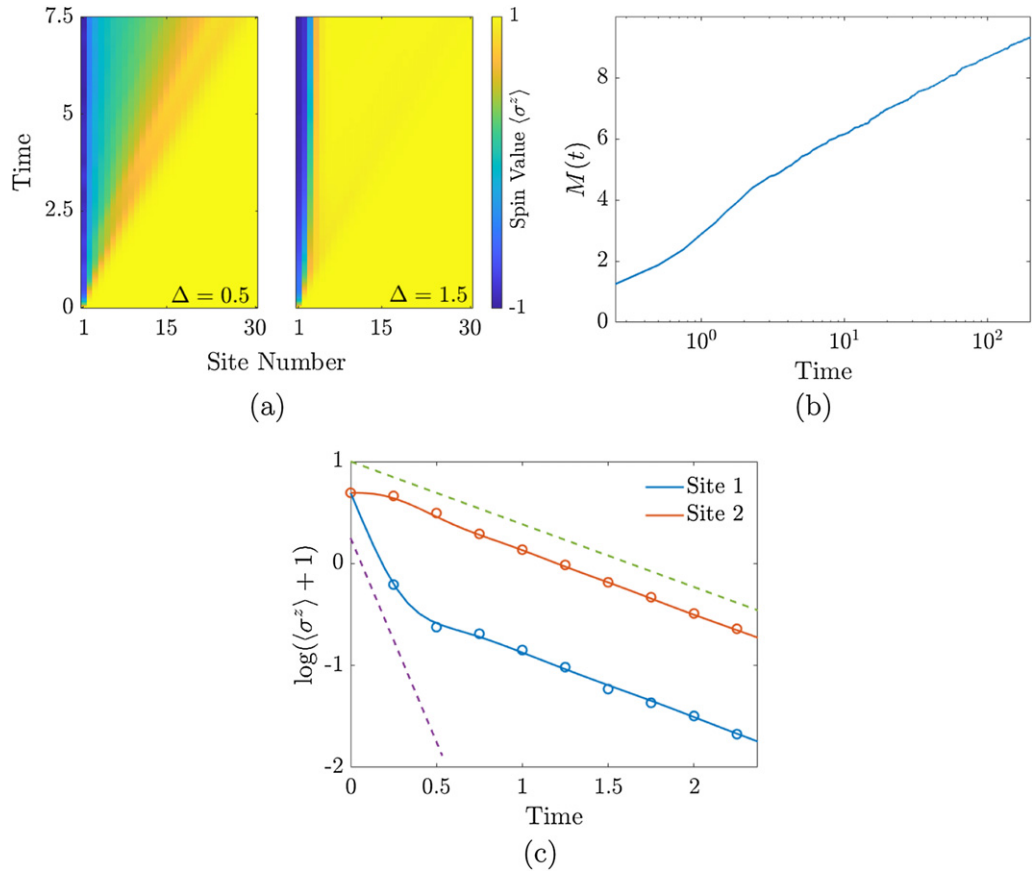

Figure 2. Domain wall formation and spin loss. (a) Magnetization along the chain as a function of time for an initially fully polarized state with $\Gamma = 0.5$. For $\Delta = 0.5$ the initial state rapidly decays to the vacuum state ρ_∞, while for $\Delta = 1.5$ the system forms a meta-stable domain wall which decays exponentially slowly. (b) The total spin lost, $M(t)$, by a 30 site system with $\Gamma = 0.5$ and $\Delta = 1.5$. This is logarithmic in time as a result of the domain wall preventing spin from leaking out. (c) The spin decay on the first and second sites in 10 (solid) and 30 (circles) site systems with $\Delta = 1.5$, $\Gamma = 0.5$. We also plot the infinite chain 0 and 1 top-magnon decay rates in purple and green respectively for comparison. The larger value of Γ than in the rest of the discussion was chosen to see non-trivial dynamics in numerically accessible time-scales.

4.3. Boundary bound states and domain wall formation in the easy-axis regime

In the second setup we consider the case where the system is initialized in a highly excited, i.e. maximally polarized (all spins-up) state. In this case, due to the structure of the eigenstates of $\hat{\mathcal{L}}$, we need only consider eigenstates with $m_L = m_R = m$. In order to study the dynamics we now focus on the most stable (maximum real part) eigenvalues in the *m top-magnon* sector, corresponding to spin-down excitations on top of the all spins-up state. The Bethe equations for top-magnons can be obtained from equation (16) by replacing $\Gamma \to -\Gamma$ in the sector with m magnons.

Focusing on the easy-axis, $\Delta > 1$, regime, we show that in the m top-magnon sector states with $\lim_{N\to\infty} \Im(k_j) > 0$, which are localized at the boundary appear and are the most stable. For these *bound* states the m top-magnon Bethe equations can be easily solved in the $N \to \infty$ limit, since $e^{ik_j N} \to 0$. A recursive solution of

$$\exp(-ik_j) + \exp(ik_{j-1}) = 2\Delta, \qquad \exp(-ik_1) = \Delta + 2i\Gamma, \tag{19}$$

gives an appealingly simple result for the leading Liouvillian eigenvalues in the m top-magnon sector,

$$\lambda_m = -2i(\exp(ik_m) - \exp(-ik_m^*)). \tag{20}$$

Physically this means that the first top-magnon with momentum k_1 is localized near the loss site, while the jth top-magnon is recursively bound to the $(j-1)$st. Importantly, we can show that as the number of top-magnons is increased they become exponentially stabilized, i.e. $\lim_{m\to\infty} \mathrm{Re}\,\lambda_m = 0$. In turn, this implies that exponentially large times (in m) are needed for the loss site to dissipate the state with m top-magnons. More details can be found in appendix D or alternatively [118].

The existence of these boundary bound states has intriguing physical consequences. It results in domain wall formation if the system is initialized in the maximally polarized state. Naively one might think that

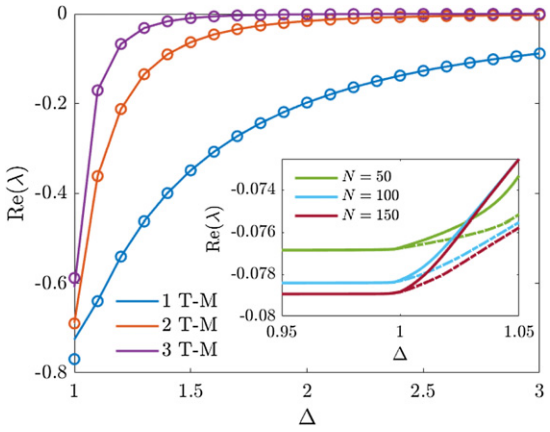

Figure 3. The eigenvalues with maximum real part of $\hat{\mathcal{L}}$ when $N \to \infty$ (circles) from equation (20) for $\Delta > 1$ compared with a 50 site system (line) for 1, 2 and 3 top-magnon sectors at $\Gamma = 0.01$. The inset shows the largest (solid line) and second largest (dashed line) real part of the eigenvalues of the Liouvillian in the one top-magnon sector for different N at $\Gamma = 0.01$. We see a cusp forming with increasing N close to $\Delta = 1$ indicating the dynamical dissipative phase transition in the large N limit at leading order in Γ.

such a state is the most unstable, however tDMRG simulations, as shown in figure 2(a), in the $\Delta > 1$ regime reveal that the total spin leaking out of the system increases only *logarithmically* with time (see figure 2(b)). This can be understood as a consequence of the exponential stability of the boundary bound states. Namely, that exponentially long times (in m) are required for the loss site to remove all the states with m down-turned spins. Moreover, in figure 2(c) we show that the dynamics of magnetization close to the spin loss site is well described by the decay rates of boundary top-magnons. On the other hand the decay of the maximally polarized state in the $\Delta < 1$ regime is very rapid (figure 2(a)), and the total loss of magnetization increases linearly with time. There have recently been a number of studies addressing the dynamics of domain walls in integrable [79–81, 83] and nonintegrable [82] systems without dissipation. While the ballistic expansion in the $\Delta < 1$ regime is well understood, the domain wall freezing was analytically unresolved.

The existence of boundary bound states also has profound consequences on the spectral properties of $\hat{\mathcal{L}}$. It results in a dissipative phase transition (shown in figure 3). In contrast to standard dissipative phase transitions [75], the stationary state remains the same (all spins-down). The phase transition rather happens in all sectors of the relaxation spectrum. At leading order in Γ as $N \to \infty$ the transition occurs at $\Delta = 1$. This is similar to *dynamical* dissipative phase transitions [73], but the discontinuous eigenvalues that are relevant for the dynamics are not only the Liouvillian gap. This is reflected in the fact that already the short time dynamics well inside the easy-plane and easy-axis regimes are qualitatively different (see figure 2(a)). The discontinuity is shown in figure 3 where, by taking small Γ, we can see non-analyticity in eigenvalues in three different top-magnon sectors at $\Delta = 1$. This is characteristic of all sectors. The non-analyticity shown corresponds to the non-existence of boundary bound state solutions for $\Delta < 1$ for all values of Γ. More specifically, we prove the existence of $\{k_j\}$ such that $\lim_{\Delta \to 1} \frac{\mathrm{d}k_j}{\mathrm{d}\Delta} \to \infty$ for large N and small Γ, which implies the divergence in the corresponding eigenvalues. See appendix C for further details.

5. Conclusion

We have developed a framework for diagonalizing quantum Liouvillians with integrable system Hamiltonians and dissipative loss. We demonstrate the utility of our method in an example of the Heisenberg *XXZ* spin chain with boundary loss. The method allows us to directly identify phase transitions in the Liouvillian spectrum and calculate the Liouvillian gap. This led us to observe two intriguing physical phenomena, namely domain wall formation, and a dissipative phase transition, which we link to the existence of boundary bound top-magnons. Such remarkable phenomena could occur in other models with localized loss, e.g. 1D Hubbard and interacting bosons in 1D [2], which can be studied analytically with our method.

A number of questions remain open. The first natural extension of our results is directly calculating the full eigenstates of the quantum Liouvillian. We also envisage using the thermodynamic Bethe ansatz [119, 120] to explore the decay of states with a finite density of excitations, and the connection with boundary states [121, 122] and strong edge modes [123] in closed systems. Additionally, the Liouvillian

spectrum exhibits a multi-band structure in the Ising limit, $\Delta \to \infty$, (see figure 4 of appendices), the ramifications of which remain unexplored.

More generally our method can be applied to a number of physically relevant systems that are quantitatively very different from the example studied here. We discuss these further in section 3. Here the interest is two-fold. On one hand, judging by our example, such systems hide a plethora of interesting physical phenomena, which are yet to be uncovered. On the other hand they describe realistic experimental setups and therefore provide an indispensable tool for understanding future experiments.

Note Added

While nearing the completion of this manuscript a related preprint appeared [92] studying exact solutions in the Hubbard model with two-body loss.

Acknowledgments

We thank F Essler, E Ilievski, M Kiffner, C Parmee, T Prosen, J Tindall, F Tonielli, and A Ziolkowska for useful discussions. We are in particularly indebted to T Prosen for suggesting the original problem that led to this study. We performed our calculations using Matrix Product State methods adapted using the Tensor Network Theory library [124] and run these on the University of Oxford Advanced Research Computing (ARC) facility [125]. BB, CB and DJ acknowledge funding from EPSRC programme grant EP/P009565/1, EPSRC National Quantum Technology Hub in Networked Quantum Information Technology (EP/M013243/1), and the European Research Council under the European Union's Seventh Framework Programme (FP7/2007–2013)/ERC Grant Agreement No. 319286, Q-MAC.

Appendices

In these appendices we provide the discussion of technical details that were omitted from the main text. In the first section we construct the eigenstates of the Liouvillian. In the second and third sections we provide details on the calculation of the Liouvillian gap, and the results related to the boundary magnons, respectively. We also plot in figure 4 the full Liouvillian spectrum for different values of anisotropy Δ which shows the formation of intriguing band structure in the Ising, $\Delta \to \infty$ limit.

Appendix A. Eigenstates of the boundary loss *XXZ* Liouvillian

In this section we will construct the right eigenstates of the Liouvillian

$$\hat{\mathcal{L}} = -\mathrm{i}(H \otimes \mathbb{1} - \mathbb{1} \otimes H^{\mathrm{T}}) + \sum_k \left(2L_\mu \otimes L_\mu^* - L_\mu^\dagger L_\mu \otimes \mathbb{1} - \mathbb{1} \otimes (L_\mu^\dagger L_\mu)^{\mathrm{T}}\right). \tag{A.1}$$

In the case of the *XXZ* chain with a single loss at the first site. First of all, we will remind the reader of the basic structure of Bethe eigenstates, which will then serve to construct the eigenstates of the Liouvillian. The eigenstate of the Hamiltonian

$$\tilde{H} = -\mathrm{i}H_{XXZ} - 4\Gamma\sigma_1^+\sigma_1^-, \tag{A.2}$$

pertaining to the energy $E_{\phi_\eta^a}$ reads

$$|\phi_\eta^a\rangle = \sum_{1\leqslant x_1<\ldots<x_a\leqslant n} f_{a,\eta}(x_1,\ldots,x_a)|x_1,\ldots,x_a\rangle. \tag{A.3}$$

Here the set of $\{x_j\}$ indicate the positions of spin-up excitations while the label a corresponds to a given total magnetisation. Finally η labels the state within this sector. In terms of Bethe roots $\{k_j\}$, the wave function reads

$$f(x_1,\ldots,x_m) = \sum_P \varepsilon_P A(k_1,\ldots,k_m)\mathrm{e}^{\mathrm{i}(k_1x_1+\ldots k_mx_m)} \tag{A.4}$$

$$A(k_1,\ldots,k_m) = \prod_{j=1}^m (\Delta\mathrm{e}^{-\mathrm{i}k_jN} - \mathrm{e}^{-\mathrm{i}(N+1)k_j}) \prod_{1\leqslant j<l\leqslant m} B(-k_j,k_l)\mathrm{e}^{-\mathrm{i}k_l} \tag{A.5}$$

$$B(k,k') = (1-2\Delta\mathrm{e}^{\mathrm{i}k'} + \mathrm{e}^{\mathrm{i}(k+k')})(1-2\Delta\mathrm{e}^{-\mathrm{i}k} + \mathrm{e}^{\mathrm{i}(k'-k)}), \tag{A.6}$$

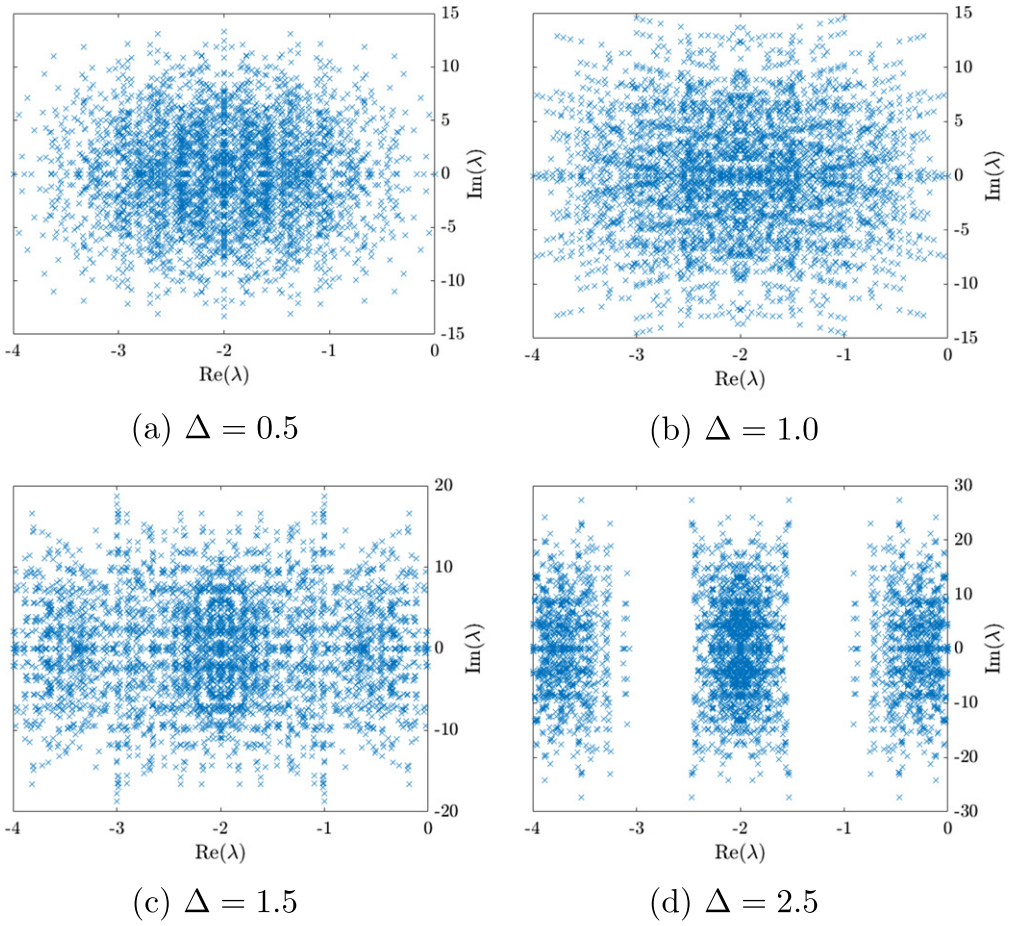

Figure 4. Full spectrum for a six site system with $\Gamma = 0.5$ at various Δ. We see the emergence of band structure forming as Δ increased. This corresponds to different subspaces of the Hilbert space decaying in separate stages. Note that similar band formation occurs in the quantum Zeno [126–129] limit of taking $\Gamma \to \infty$ for any Δ. However, here we fix $\Gamma = 0.5$ and increase Δ. In both cases the bands appear at $\mathrm{Re}(\lambda) = 0, 4\Gamma, 8\Gamma$. With Γ fixed the band locations remain finite, whereas when $\Gamma \to \infty$ the band locations also become infinite.

where the summation is performed over all permutations and negations of $\{k_j\}$, and ε_P changes sign with each such *mutation*.

We then use the triangular form for the Liouvillian, i.e. that

$$\mathcal{L} : \mathcal{M}^a \otimes \mathcal{M}^b \to \left(\mathcal{M}^a \otimes \mathcal{M}^b\right) \oplus \left(\mathcal{M}^{a-1} \otimes \mathcal{M}^{b-1}\right), \tag{A.7}$$

where $\mathcal{M}^a$ is the subspace with magnetization a, to make the ansatz that the eigenstate of $\mathcal{L}$ with eigenvalue $E_{\phi_\eta^a} + E^*_{\phi_\zeta^b}$ is given by

$$|\Phi^{a,b}_{\eta,\zeta}\rangle = |\phi^a_\eta\rangle\overline{|\phi^b_\zeta\rangle} + \sum_{\mu=1}^{\min\{a,b\}} \sum_{i,j} B_\mu(i,j)|\phi_i^{a-\mu}\rangle\overline{|\phi_j^{b-\mu}\rangle}. \tag{A.8}$$

Substituting this gives the recurrence relation

$$B_\mu(i,j) = \frac{8\Gamma}{E_\mu(i,j)} \sum_{p,q} B_{\mu-1}(p,q)\Sigma_{a-\mu+1}(p,i)\Sigma_{b-\mu+1}(q,j)^*, \qquad B_0(i,j) = \delta_{i,\eta}\delta_{j,\zeta} \tag{A.9}$$

for $\mu = 1, \ldots, \min\{a,b\}$, where we defined

$$E_\mu(i,j) = (E_{\phi^a_\eta} + E^*_{\phi^b_\zeta}) - (E_{\phi_i^{a-\mu}} + E^*_{\phi_j^{b-\mu}}) \tag{A.10}$$

$$\Sigma_m(p,i) = \sum_{\{x_2,\ldots x_m\},\ x_2>1} f_{m,p}(1,x_2,\ldots x_m) f_{m-1,i}(x_2,\ldots,x_m). \tag{A.11}$$

In general, this recursion relation is significantly more complex than computing the Bethe states of $\tilde{H}$. It does however provide an insight into the structure of the eigenstates. We also note that one of the main

powers of Bethe ansatz lies in the thermodynamics and that efficient calculations might still be possible in such a limit.

Appendix B. Thermodynamic limit of the leading decay rates

B.1. Easy plane, $\Delta \leqslant 1$, regime

Here we will study the solutions of the Bethe equations that have purely real momenta in the thermodynamic limit. These solutions can be physically understood as free magnons that live in the bulk of the system and only experience the effects of other magnons and the boundary in sub-leading order $1/N$. To do this we start with the logarithmic form of the Bethe equations,

$$2\mathrm{i}k_j = \frac{1}{N}\left(\sum_{i\neq j}\log\left[S(\mathrm{e}^{\mathrm{i}k_j},\mathrm{e}^{\mathrm{i}k_i})\right]\right) - \frac{2\mathrm{i}\pi I_j}{N}. \tag{B.1}$$

In order to simplify discussion we focus on the single magnon case, though the solutions for m magnons are also straightforward in the above discussed limit,

$$2\mathrm{i}k = \frac{\Omega(\mathrm{e}^{\mathrm{i}k})}{N} - \frac{2\mathrm{i}\pi I_1}{N}, \tag{B.2}$$

We denote by

$$\Omega(a) = \log\left(\frac{(a\Delta-1)(-1+a(\Delta-2\mathrm{i}\Gamma))}{(a-\Delta)(a+2\mathrm{i}\Gamma-\Delta)}\right), \tag{B.3}$$

and expand the momenta k as the power series in $1/N$, $k = k^{(0)} + 1/Nk^{(1)} + \cdots$, which we truncate at the order $\mathcal{O}(1/N^3)$. It is important to distinguish the cases when the integer I_1 is finite and when it is of the order of the system size N or close to N. Since the leading decay mode corresponds to the latter case, we make the transformation $I_1 \to N - I_1$ and focus on finite I_1.

Expanding (B.2) is straightforward, as is solving it order by order. We arrive at,

$$\begin{aligned} k = -\pi + \frac{1}{N}\pi I_1 + \frac{1}{N^2}\pi I_1\left(-\frac{1}{-2i\Gamma+\Delta+1} - \frac{1}{\Delta+1} + 1\right) \\ + \frac{1}{N^3}\frac{\pi I_1\left(-2\mathrm{i}\Gamma\Delta+\Delta^2-1\right)^2}{(\Delta+1)^2(-2\mathrm{i}\Gamma+\Delta+1)^2} + \mathcal{O}\left(\frac{1}{N^4}\right). \end{aligned} \tag{B.4}$$

Let us recall the eigenvalue equation,

$$\lambda_{i,j} = -4\mathrm{i}(\cos(k_i) - \cos(k_j^*)), \tag{B.5}$$

where i, j distinguishes different solutions given by I_1 in (B.4). The gap comes from an off-diagonal state composed of the vacuum state and the single spin-up excitation, i.e. $k_i = 0, k_j = k(I_1 = 1)$. Setting this gives the gap equation in the main text.

B.2. Easy axis, $\Delta > 1$, regime

Here we consider solutions which are purely imaginary in the thermodynamic limit. To obtain the form of the gap, R, we consider the single magnon Bethe equation,

$$\mathrm{e}^{2\mathrm{i}kN}(\Delta-\mathrm{e}^{\mathrm{i}k})((-\Delta+2\mathrm{i}\Gamma)+\mathrm{e}^{\mathrm{i}k}) - (-1+\Delta\mathrm{e}^{\mathrm{i}k})(1+(-\Delta+2\mathrm{i}\Gamma)\mathrm{e}^{\mathrm{i}k}) = 0. \tag{B.6}$$

We make the ansatz $k = \mathrm{i}\log\left(\frac{1}{\Delta}\right) - a_1\Delta^{-2N} + o(\Delta^{-2N})$, and expand (B.6) to find,

$$0 = (\Delta^2-1)(-2\mathrm{i}\Gamma+\Delta^2-1) - 2\Gamma\Delta a_1 + \mathcal{O}(\Delta^{-2N}), \tag{B.7}$$

which we may solve for a_1. Using (B.5) with $k_i = 0,\ k_j = \mathrm{i}\log\left(\frac{1}{\Delta}\right) - a_1\Delta^{-2N}$ gives the result in the main text.

Strictly speaking these results for both the easy axis and easy plane regime represent an upper bound on the gap, although extensive numerical evidence also shows that they are also a lower bound. We hope to prove that this is the gap by extending techniques for the isolated XXZ spin chain [130].

Appendix C. Calculation of the phase transition in the highly excited eigenstates

We will now study the one top-magnon (spin-down in a background of all spins up) sector. The single top-magnon cases correspond to setting $\Omega(a) = \log\left(\frac{(a\Delta-1)(-1+a(\Delta+2i\Gamma))}{(a-\Delta)(a-2i\Gamma-\Delta)}\right)$ in (B.2). The corresponding energies of $\tilde{H}$ are,

$$E_p = -4\Gamma - 4i(\cos(k_p) - \Delta), \tag{C.1}$$

while the eigenvalues of $\hat{\mathcal{L}}$ read,

$$\lambda_{p,p'} = E_p + E^*_{p'}. \tag{C.2}$$

We now look at the case when I_1 is finite. Numerically we observe that this corresponds to the leading decay rates in the single top-magnon sector for $\Delta < 1$ in the small Γ limit. Performing the same expansion as before, relabeling $I_1 \to p$, we obtain (now it is sufficient to look at only up to order $1/N^2$),

$$k_p = -\frac{p\pi}{N} + \frac{1}{N^2}\left[\pi p\left(-\frac{1}{-2i\Gamma+\Delta-1} + \frac{1}{1-\Delta} - 1\right)\right]. \tag{C.3}$$

We take the derivative w.r.t. to Δ of (C.2),

$$\frac{d\lambda_{p,p'}}{d\Delta} = -4i\left[-\sin(k_p)\frac{dk_p}{d\Delta} + \sin(k^*_{p'})\frac{dk^*_{p'}}{d\Delta}\right]. \tag{C.4}$$

Using (C.3) we obtain,

$$\frac{d\lambda_{p,p'}}{d\Delta} = -4i\pi^2\left(\frac{p^2-p'^2}{(1-\Delta)^2} + \frac{p^2+p'^2}{(-2i\Gamma+\Delta-1)^2}\right)\frac{1}{N^3} + O\left(\frac{1}{N^4}\right) \tag{C.5}$$

which diverges as $\Delta \to 1$ at leading order in Γ, signalling the phase transition in these highly excited states.

Appendix D. Boundary bound modes and stability of the domain wall in the easy-axis regime

In the easy-axis regime, $\Delta > 1$, an infinite number of solutions that have non-zero imaginary part in the thermodynamic limit appear, $\lim_{N\to\infty} \Im(k_j) \neq 0$. In contrast, in the easy-plane regime we observe that only a finite number of such solutions can appear at finite $\Gamma \neq 0$.

We study the solutions with $\lim_{N\to\infty} \Im(k_j) > 0$. These correspond to top-magnons localized at the boundary loss site, which we refer to as boundary bound modes. More specifically, we may solve the m top-magnon Bethe equations in the $N \to \infty$ limit by observing that $e^{ik_jN} \to 0$. Focusing on the top-magnon boundary bound modes, we arrive at the following simple form of the Bethe equations in the $N \to \infty$ limit,

$$\left(1 + e^{ik_j}(-\Delta - 2i\Gamma)\right)\prod_{i\neq j}\left(-2\Delta e^{ik_j} + e^{i(k_j-k_i)} + 1\right)\left(e^{i(k_j+k_i)} - 2\Delta e^{ik_j} + 1\right) = 0. \tag{D.1}$$

These may be recursively solved,

$$\exp(-ik_j) + \exp(ik_{j-1}) = 2\Delta, \qquad \exp(-ik_1) = \Delta + 2i\Gamma. \tag{D.2}$$

Physically, this means that the k_1 top-magnon is localized at the loss site, whereas the jth top-magnon is bound to the $(j-1)$st one. This characterises a domain wall state.

We will now show that the real part of the eigenvalues decay exponentially with top-magnon number m. First, we decompose the equations for energies (C.1) as

$$E_m = -4\Gamma - 4i\sum_{i=1}^{m}\left(\frac{1}{2}\left(\exp(ik_i) + \exp(-ik_i)\right) - \Delta\right). \tag{D.3}$$

Regrouping the terms, we simply get

$$E_m = -2i\left(\exp(ik_m) - \Delta\right). \tag{D.4}$$

In order to demonstrate stability it is sufficient to show that the imaginary part of $\exp(ik_m)$ goes to 0 in the limit of large top-magnon number, $m \to \infty$. Let us write recursion relations for $\exp(ik_m)$

$$\begin{aligned}\exp(ik_{2j+1}) &= -\frac{2\Delta - \exp(ik_{2j-1})}{1 - 2\Delta(2\Delta - \exp(ik_{2j-1}))},\\ \exp(ik_1) &= (\Delta + 2i\Gamma)^{-1}, \quad \exp(ik_2) = \frac{\Delta - 2i\Gamma}{2\Delta(\Delta - 2i\Gamma) - 1}.\end{aligned} \tag{D.5}$$

Solving for the stationary value of recursion, $z = \exp(ik_{2j+1}) = \exp(ik_{2j-1})$, we obtain two *real* solutions,

$$z_1 = \Delta - \sqrt{-1 + \Delta^2}, \qquad z_2 = \Delta + \sqrt{-1 + \Delta^2}, \tag{D.6}$$

with the stable point being z_1. We numerically observe that this fixed point is converged to for any initial value of $\Delta > 1$ and Γ. The decay of the most stable eigenvalue $\lambda_m = 2\,\mathrm{Re}(E_m)$ is thus exponential in top-magnon number m, demonstrating the stability of the domain wall.

ORCID iDs

Berislav Buča https://orcid.org/0000-0003-3119-412X
Cameron Booker https://orcid.org/0000-0003-1038-3220

References

[1] Gross C and Bloch I 2017 Quantum simulations with ultracold atoms in optical lattices *Science* **357** 995–1001
[2] Lewenstein M, Sanpera A, Ahufinger V, Damski B, Sen A and Sen U 2007 Ultracold atomic gases in optical lattices: mimicking condensed matter physics and beyond *Adv. Phys.* **56** 243–379
[3] Zezyulin D A, Konotop V V, Barontini G and Ott H 2012 Macroscopic Zeno effect and stationary flows in nonlinear waveguides with localized dissipation *Phys. Rev. Lett.* **109** 020405
[4] Fitzpatrick M, Sundaresan N M, Li A C Y, Koch J and Houck A A 2017 Observation of a dissipative phase transition in a one-dimensional circuit QED lattice *Phys. Rev.* X **7** 011016
[5] Tangpanitanon J, Bastidas V M, Al-Assam S, Roushan P, Jaksch D and Angelakis D G 2016 Topological pumping of photons in nonlinear resonator arrays *Phys. Rev. Lett.* **117** 213603
[6] Tangpanitanon J, Clark S R, Bastidas V M, Fazio R, Jaksch D and Angelakis D G 2019 Hidden order in quantum many-body dynamics of driven-dissipative nonlinear photonic lattices *Phys. Rev.* A **99** 043808
[7] Wolff S, Sheikhan A and Kollath C 2016 Dissipative time evolution of a chiral state after a quantum quench *Phys. Rev.* A **94** 043609
[8] Zhang Q, Lou M, Li X, Reno J L, Pan W, Watson J D, Manfra M J and Kono J 2016 Collective non-perturbative coupling of 2D electrons with high-quality-factor terahertz cavity photons *Nat. Phys.* **12** 1005–11
[9] Scalari G *et al* 2012 Ultrastrong coupling of the cyclotron transition of a 2D electron gas to a THz metamaterial *Science* **335** 1323–6
[10] Halati C M, Sheikhan A, Ritsch H and Kollath C 2020 Numerically exact treatment of many-body self-organization in a cavity *Phys. Rev. Lett.* **125** 093604
[11] Schlawin F, Cavalleri A and Jaksch D 2019 Cavity-mediated electron–photon superconductivity *Phys. Rev. Lett.* **122** 133602
[12] Fröml H, Muckel C, Kollath C, Chiocchetta A and Diehl S 2019 Ultracold quantum wires with localized losses: many-body quantum Zeno effect *Phys. Rev.* B **101** 144301
[13] Lebrat M, Häusler S, Fabritius P, Husmann D, Corman L and Esslinger T 2019 Quantized conductance through a spin-selective atomic point contact *Phys. Rev. Lett.* **123** 193605
[14] Mitrano M *et al* 2014 Pressure-dependent relaxation in the photoexcited Mott insulator ET–F_2TCNQ: influence of hopping and correlations on quasiparticle recombination rates *Phys. Rev. Lett.* **112** 117801
[15] De Franceschi S, Kouwenhoven L, Schönenberger C and Wernsdorfer W 2010 Hybrid superconductor-quantum dot devices *Nat. Nanotechnol.* **5** 703–11
[16] Prosen T 2011 Open *XXZ* spin chain: nonequilibrium steady state and a strict bound on ballistic transport *Phys. Rev. Lett.* **106** 217206
[17] Prosen T 2011 Exact nonequilibrium steady state of a strongly driven open *XXZ* chain *Phys. Rev. Lett.* **107** 137201
[18] Popkov V and Prosen T 2015 Infinitely dimensional lax structure for the one-dimensional Hubbard model *Phys. Rev. Lett.* **114** 127201
[19] Ilievski E 2014 Exact solutions of open integrable quantum spin chains (arXiv:1410.1446)
[20] Ilievski E 2017 Dissipation-driven integrable fermionic systems: from graded Yangians to exact nonequilibrium steady states *SciPost Phys.* **3** 031
[21] Ilievski E and Prosen T 2014 Exact steady state manifold of a boundary driven spin-1 Lai–Sutherland chain *Nucl. Phys.* B **882** 485–500
[22] Ilievski E and Žunkovič B 2014 Quantum group approach to steady states of boundary-driven open quantum systems *J. Stat. Mech.* P01001
[23] Žunkovič B 2014 Closed hierarchy of correlations in Markovian open quantum systems *New J. Phys.* **16** 013042
[24] Lenarčič Z and Prosen T 2015 Exact asymptotics of the current in boundary-driven dissipative quantum chains in large external fields *Phys. Rev.* E **91** 030103
[25] Karevski D, Popkov V and Schütz G M 2013 Exact matrix product solution for the boundary-driven Lindblad *XXZ* chain *Phys. Rev. Lett.* **110** 047201
[26] Popkov V and Schütz G M 2017 Solution of the Lindblad equation for spin helix states *Phys. Rev.* E **95** 042128
[27] Yuge T and Sugita A 2015 A perturbative method for nonequilibrium steady state of open quantum systems *J. Phys. Soc. Japan* **84** 014001
[28] Popkov V, Prosen T and Zadnik L 2019 Exact nonequilibrium steady state of open *XXZ*/*XYZ* spin-1/2 chain with Dirichlet boundary conditions *Phys. Rev. Lett.* **124** 160403
[29] Vanicat M, Zadnik L and Prosen T 2018 Integrable trotterization: local conservation laws and boundary driving *Phys. Rev. Lett.* **121** 030606
[30] Buča B and Prosen T 2014 Exactly solvable counting statistics in open weakly coupled interacting spin systems *Phys. Rev. Lett.* **112** 067201
[31] Nigro D 2020 Complexity of the steady state of weakly symmetric open quantum lattices *Phys. Rev.* A **101** 022109

[32] Prosen T 2015 Matrix product solutions of boundary driven quantum chains *J. Phys. A: Math. Theor.* **48** 373001
[33] Diehl S, Micheli A, Kantian A, Kraus B, Büchler H P and Zoller P 2008 Quantum states and phases in driven open quantum systems with cold atoms *Nat. Phys.* **4** 878–83
[34] Buča B and Prosen T 2018 Strongly correlated non-equilibrium steady states with currents—quantum and classical picture *Eur. Phys. J. Spec. Top.* **227** 421–44
[35] Bernard D and Jin T 2019 Open quantum symmetric simple exclusion process *Phys. Rev. Lett.* **123** 080601
[36] Žnidarič M 2011 Spin transport in a one-dimensional anisotropic Heisenberg model *Phys. Rev. Lett.* **106** 220601
[37] Žnidarič M 2014 Exact large-deviation statistics for a nonequilibrium quantum spin chain *Phys. Rev. Lett.* **112** 040602
[38] Žnidarič M 2010 Exact solution for a diffusive nonequilibrium steady state of an open quantum chain *J. Stat. Mech.* L05002
[39] Prosen T 2008 Third quantization: a general method to solve master equations for quadratic open Fermi systems *New J. Phys.* **10** 043026
[40] Prosen T and Seligman T H 2010 Quantization over boson operator spaces *J. Phys. A: Math. Theor.* **43** 392004
[41] Manzano D, Chuang C and Cao J 2016 Quantum transport in *d* dimensional lattices *New J. Phys.* **18** 043044
[42] Monthus C 2017 Boundary-driven Lindblad dynamics of random quantum spin chains: strong disorder approach for the relaxation, the steady state and the current *J. Stat. Mech.* 043303
[43] Krapivsky P L, Mallick K and Sels D 2019 Free fermions with a localized source *J. Stat. Mech.* 113108
[44] Carollo F, Garrahan J P, Lesanovsky I and Pérez-Espigares C 2017 Fluctuating hydrodynamics, current fluctuations, and hyperuniformity in boundary-driven open quantum chains *Phys. Rev.* E **96** 052118
[45] Budich J C, Zoller P and Diehl S 2015 Dissipative preparation of Chern insulators *Phys. Rev.* A **91** 042117
[46] Iemini F, Rossini D, Fazio R, Diehl S and Mazza L 2016 Dissipative topological superconductors in number-conserving systems *Phys. Rev.* B **93** 115113
[47] Medvedyeva M V and Kehrein S 2014 Power-law approach to steady state in open lattices of noninteracting electrons *Phys. Rev.* B **90** 205410
[48] Guo C and Poletti D 2017 Solutions for bosonic and fermionic dissipative quadratic open systems *Phys. Rev.* A **95** 052107
[49] Medvedyeva M V, Essler F H L and Tcv P 2016 Exact Bethe ansatz spectrum of a tight-binding chain with dephasing noise *Phys. Rev. Lett.* **117** 137202
[50] Rowlands D A and Lamacraft A 2018 Noisy spins and the Richardson-Gaudin model *Phys. Rev. Lett.* **120** 090401
[51] Ziolkowska A A and Essler F H L 2020 Yang–Baxter integrable Lindblad equations *SciPost Phys.* **8** 44
[52] Ziolkowska A A 2019 personal communication
[53] Shibata N and Katsura H 2019 Dissipative quantum Ising chain as a non-Hermitian Ashkin–Teller model *Phys. Rev.* B **99** 224432
[54] Shibata N and Katsura H 2019 Dissipative spin chain as a non-Hermitian Kitaev ladder *Phys. Rev.* B **99** 174303
[55] Maity S, Bandyopadhyay S, Bhattacharjee S and Dutta A 2020 Growth of mutual information in a quenched one-dimensional open quantum many-body system *Phys. Rev.* B **101** 180301
[56] Lerma-Hernández S, Rubio-García A and Dukelsky J 2020 Trigonometric SU(N) Richardson–Gaudin models and dissipative multi-level atomic systems (arXiv:2005.05155)
[57] Essler F H L and Piroli L 2020 Integrability of 1D Lindbladians from operator-space fragmentation (arXiv:2009.11745)
[58] van Caspel M and Gritsev V 2018 Symmetry-protected coherent relaxation of open quantum systems *Phys. Rev.* A **97** 052106
[59] Bastianello A, Nardis J D and Luca A D 2020 Generalised hydrodynamics with dephasing noise *Phys. Rev.* B **102** 161110
[60] Lange F, Lenarčič Z and Rosch A 2017 Pumping approximately integrable systems *Nat. Commun.* **8** 15767
[61] Lenarčič Z, Lange F and Rosch A 2018 Perturbative approach to weakly driven many-particle systems in the presence of approximate conservation laws *Phys. Rev.* B **97** 024302
[62] Banchi L, Burgarth D and Kastoryano M J 2017 Driven quantum dynamics: will it blend? *Phys. Rev.* X **7** 041015
[63] Tonielli F, Fazio R, Diehl S and Marino J 2019 Orthogonality catastrophe in dissipative quantum many-body systems *Phys. Rev. Lett.* **122** 040604
[64] Kuhr S 2016 Quantum-gas microscopes: a new tool for cold-atom quantum simulators *Natl Sci. Rev.* **3** 170–2
[65] Damanet F, Mascarenhas E, Pekker D and Daley A J 2019 Controlling quantum transport via dissipation engineering *Phys. Rev. Lett.* **123** 180402
[66] Barontini G, Labouvie R, Stubenrauch F, Vogler A, Guarrera V and Ott H 2013 Controlling the dynamics of an open many-body quantum system with localized dissipation *Phys. Rev. Lett.* **110** 035302
[67] Wolff S, Sheikhan A, Diehl S and Kollath C 2020 Nonequilibrium metastable state in a chain of interacting spinless fermions with localized loss *Phys. Rev.* B **101** 075139
[68] Buča B and Prosen T 2012 A note on symmetry reductions of the Lindblad equation: transport in constrained open spin chains *New J. Phys.* **14** 073007
[69] Buča B and Prosen T 2017 Charge and spin current statistics of the open Hubbard model with weak coupling to the environment *Phys. Rev.* E **95** 052141
[70] Mendoza-Arenas J J, Mitchison M T, Clark S R, Prior J, Jaksch D and Plenio M B 2014 Transport enhancement from incoherent coupling between one-dimensional quantum conductors *New J. Phys.* **16** 053016
[71] Tonielli F, Chakraborty N, Grusdt F and Marino J 2020 Ramsey interferometry of non-Hermitian quantum impurities *Phys. Rev. Res.* **2** 032003
[72] Dolgirev P E, Marino J, Sels D and Demler E 2020 Non-Gaussian correlations imprinted by local dephasing in fermionic wires *Phys. Rev.* B **102** 100301
[73] Horstmann B, Cirac J I and Giedke G 2013 Noise-driven dynamics and phase transitions in fermionic systems *Phys. Rev.* A **87** 012108
[74] Can T, Oganesyan V, Orgad D and Gopalakrishnan S 2019 Spectral gaps and midgap states in random quantum master equations *Phys. Rev. Lett.* **123** 234103
[75] Kessler E M, Giedke G, Imamoglu A, Yelin S F, Lukin M D and Cirac J I 2012 Dissipative phase transition in a central spin system *Phys. Rev.* A **86** 012116
[76] Bhaseen M J, Mayoh J, Simons B D and Keeling J 2012 Dynamics of nonequilibrium Dicke models *Phys. Rev.* A **85** 013817
[77] Marcuzzi M, Levi E, Diehl S, Garrahan J P and Lesanovsky I 2014 Universal nonequilibrium properties of dissipative rydberg gases *Phys. Rev. Lett.* **113** 210401
[78] Casteels W, Fazio R and Ciuti C 2017 Critical dynamical properties of a first-order dissipative phase transition *Phys. Rev.* A **95** 012128

[79] Collura M, De Luca A and Viti J 2018 Analytic solution of the domain-wall nonequilibrium stationary state *Phys. Rev.* B **97** 081111
[80] Gamayun O, Miao Y and Ilievski E 2019 Domain-wall dynamics in the Landau–Lifshitz magnet and the classical-quantum correspondence for spin transport *Phys. Rev.* B **99** 140301
[81] Misguich G, Pavloff N and Pasquier V 2019 Domain wall problem in the quantum *XXZ* chain and semiclassical behavior close to the isotropic point *SciPost Phys* **7** 025
[82] Medenjak M and De Nardis J 2020 Domain wall melting in spin-1 *XXZ* chains *Phys. Rev.* B **101** 081411
[83] Collura M, De Luca A, Calabrese P and Dubail J 2020 Domain-wall melting in the spin-1/2 *XXZ* spin chain: emergent Luttinger liquid with fractal quasi-particle charge (arXiv:2001.04948)
[84] Breuer H P, Petruccione F *et al* 2002 *The Theory of Open Quantum Systems* (Oxford: Oxford University Press)
[85] Gardiner C, Zoller P and Zoller P 2004 *Quantum Noise: A Handbook of Markovian and Non-Markovian Quantum Stochastic Methods with Applications to Quantum Optics* (Berlin: Springer)
[86] Torres J M 2014 Closed-form solution of Lindblad master equations without gain *Phys. Rev.* A **89** 052133
[87] Briegel H-J and Englert B-G 1993 Quantum optical master equations: the use of damping bases *Phys. Rev.* A **47** 3311–29
[88] Bethe H 1931 Zur theorie der Metalle *Z. Phys.* **71** 205–26
[89] Korepin V E, Bogoliubov N M and Izergin A G 1997 *Quantum Inverse Scattering Method and Correlation Functions* vol 3 (Cambridge: Cambridge University Press)
[90] Parmee C D and Cooper N R 2018 Phases of driven two-level systems with nonlocal dissipation *Phys. Rev.* A **97** 053616
[91] Parmee C D and Cooper N R 2019 Decay rates and energies of free magnons and bound states in dissipative *XXZ* chains *Phys. Rev.* A **99** 063615
[92] Nakagawa M, Kawakami N and Ueda M 2020 Exact Liouvillian spectrum of a one-dimensional dissipative Hubbard model arXiv:2003.14202
[93] Deguchi T and Yue R 1997 Exact solutions of 1-D Hubbard model with open boundary conditions and the conformal dimensions under boundary magnetic fields arXiv:cond-mat/9704138
[94] Dürr S, García-Ripoll J J, Syassen N, Bauer D M, Lettner M, Cirac J I and Rempe G 2009 Lieb–Liniger model of a dissipation-induced Tonks–Girardeau gas *Phys. Rev.* A **79** 023614
[95] Jaksch D, Gardiner S A, Schulze K, Cirac J I and Zoller P 2001 Uniting Bose–Einstein condensates in optical resonators *Phys. Rev. Lett.* **86** 4733–6
[96] Baumann K, Guerlin C, Brennecke F and Esslinger T 2010 Dicke quantum phase transition with a superfluid gas in an optical cavity *Nature* **464** 1301–6
[97] Dalla Torre E G, Otterbach J, Demler E, Vuletic V and Lukin M D 2013 Dissipative preparation of spin squeezed atomic ensembles in a steady state *Phys. Rev. Lett.* **110** 120402
[98] Dogra N, Landini M, Kroeger K, Hruby L, Donner T and Esslinger T 2019 Dissipation-induced structural instability and chiral dynamics in a quantum gas *Science* **366** 1496–9
[99] Cosme J G, Skulte J and Mathey L 2019 Time crystals in a shaken atom-cavity system *Phys. Rev.* A **100** 053615
[100] Jamison A O, Plotkin-Swing B and Gupta S 2014 Advances in precision contrast interferometry with Yb Bose–Einstein condensates *Phys. Rev.* A **90** 063606
[101] Kohler S and Sols F 2002 Oscillatory decay of a two-component Bose–Einstein condensate *Phys. Rev. Lett.* **89** 060403
[102] Seibold K, Rota R and Savona V 2020 Dissipative time crystal in an asymmetric nonlinear photonic dimer *Phys. Rev.* A **101** 033839
[103] Graefe E M, Korsch H and Niederle A 2008 Mean-field dynamics of a non-Hermitian Bose–Hubbard dimer *Phys. Rev. Lett.* **101** 150408
[104] Lledó C, Mavrogordatos T K and Szymańska M 2019 Driven Bose–Hubbard dimer under nonlocal dissipation: a bistable time crystal *Phys. Rev.* B **100** 054303
[105] Casteels W and Wouters M 2017 Optically bistable driven-dissipative Bose–Hubbard dimer: Gutzwiller approaches and entanglement *Phys. Rev.* A **95** 043833
[106] Links J 2006 Bethe ansatz solutions of the Bose–Hubbard dimer *Symmetry, Integrability and Geometry: Methods and Applications* **2** 095
[107] Enol'skii V, Salerno M, Kostov N and Scott A 1991 Alternate quantizations of the discrete self-trapping dimer *Phys. Scr.* **43** 229
[108] Dukelsky J, Pittel S and Sierra G 2004 Colloquium: Exactly solvable Richardson–Gaudin models for many-body quantum systems *Rev. Mod. Phys.* **76** 643
[109] Prosen T and Žunkovič B 2010 Exact solution of Markovian master equations for quadratic Fermi systems: thermal baths, open XY spin chains and non-equilibrium phase transition *New J. Phys.* **12** 025016
[110] Mendoza-Arenas J J, Žnidarič M, Varma V K, Goold J, Clark S R and Scardicchio A 2019 Asymmetry in energy versus spin transport in certain interacting disordered systems *Phys. Rev.* B **99** 094435
[111] Žnidarič M, Mendoza-Arenas J J, Clark S R and Goold J 2017 Dephasing enhanced spin transport in the ergodic phase of a many-body localizable system *Ann. Phys.* **529** 1600298
[112] Mendoza-Arenas J J, Clark S R and Jaksch D 2015 Coexistence of energy diffusion and local thermalization in nonequilibrium *XXZ* spin chains with integrability breaking *Phys. Rev.* E **91** 042129
[113] Mendoza-Arenas J J, Grujic T, Jaksch D and Clark S R 2013 Dephasing enhanced transport in nonequilibrium strongly correlated quantum systems *Phys. Rev.* B **87** 235130
[114] Sklyanin E K 1988 Boundary conditions for integrable quantum systems *J. Phys. A: Math. Gen.* **21** 2375–89
[115] Alcaraz F C, Barber M N, Batchelor M T, Baxter R J and Quispel G R W 1987 Surface exponents of the quantum *XXZ*, Ashkin–Teller and Potts models *J. Phys. A: Math. Gen.* **20** 6397–409
[116] Ragoucy E 2012 Generalized coordinate Bethe ansatz for open spin chains with non-diagonal boundaries *J. Phys.: Conf. Ser.* **343** 012100
[117] Crampé N, Ragoucy E and Simon D 2010 Eigenvectors of open *XXZ* and ASEP models for a class of non-diagonal boundary conditions *J. Stat. Mech.* P11038
[118] Gochev I G 1977 Spin complexes in a bounded chain *JETP Lett.* **26** 127
[119] van Tongeren S J 2016 Introduction to the thermodynamic Bethe ansatz *J. Phys. A: Math. Theor.* **49** 323005
[120] Yang C N and Yang C P 1969 Thermodynamics of a one-dimensional system of bosons with repulsive delta-function interaction *J. Math. Phys.* **10** 1115–22
[121] Grijalva S, Nardis J D and Terras V 2019 Open *XXZ* chain and boundary modes at zero temperature *SciPost Phys.* **7** 23

[122] Nardis J D, Krajenbrink A, Doussal P L and Thiery T 2019 Delta-Bose gas on a half-line and the KPZ equation: boundary bound states and unbinding transitions *J. Stat. Mech.* 043207
[123] Fendley P 2016 Strong zero modes and eigenstate phase transitions in the XYZ/interacting Majorana chain *J. Phys. A: Math. Theor.* **49** 30LT01
[124] Al-Assam S, Clark S R and Jaksch D 2017 The tensor network theory library *J. Stat. Mech.* 093102
[125] Richards A 2015 *University of Oxford Advanced Research Computing* available from: https://doi.org/10.5281/zenodo.22558
[126] Facchi P and Pascazio S 2008 Quantum Zeno dynamics: mathematical and physical aspects *J. Phys. A: Math. Theor.* **41** 493001
[127] Facchi P and Pascazio S 2002 Quantum Zeno subspaces *Phys. Rev. Lett.* **89** 080401
[128] Zanardi P and Campos Venuti L 2014 Coherent quantum dynamics in steady-state manifolds of strongly dissipative systems *Phys. Rev. Lett.* **113** 240406
[129] Popkov V, Essink S, Presilla C and Schütz G 2018 Effective quantum Zeno dynamics in dissipative quantum systems *Phys. Rev.* A **98** 052110
[130] Koma T and Nachtergaele B 1997 The spectral gap of the ferromagnetic *XXZ*-chain *Lett. Math. Phys.* **40** 1–16